Thermodynamic and radiative properties of TiO in local thermal equilibrium and non-equilibrium conditions

Tianrui Bai, Zhi Qin & Linhua Liu

Taylor & Francis
Taylor & Francis Group

Check for updates

RESEARCH ARTICLE

Thermodynamic and radiative properties of TiO in local thermal equilibrium and non-equilibrium conditions

Tianrui Bai[a,b], Zhi Qin ![ORCID][b,c] and Linhua Liu[a,b,d]

[a]School of Energy and Power Engineering, Shandong University, Jinan, People's Republic of China; [b]Optics and Thermal Radiation Research Center, Institute of Frontier and Interdisciplinary Science, Shandong University, Qingdao, People's Republic of China; [c]School of information science and Engineering, Shandong University, Qingdao, People's Republic of China; [d]School of Energy Science and Engineering, Harbin Institute of Technology, Harbin, People's Republic of China

ABSTRACT

The thermodynamic and radiative properties of TiO in the local thermodynamic equilibrium (LTE) and non-LTE (NLTE) were investigated. Firstly, we investigated the potential energy curves of fifteen electronic states of TiO by the icMRCI + Q method with a large aug-cc-pwCV5Z-DK basis set. Then the internal partition functions, average internal energies, specific heats at temperatures from 100 to 15,000 K in the LTE and NLTE were obtained. The contributions of different states are not affected by the condition of the gas. In addition, the transition dipole moments for eight transitions and the radiative properties (absorption and emissivity) of TiO in the LTE and NLTE were obtained. The $A^3\Phi - X^3\Delta$, $B^3\Pi - X^3\Delta$ and $C^3\Delta - X^3\Delta$ transitions play a key role in the calculations of the absorption and emissivity. The absorption and emissivity in the LTE and NLTE were also calculated, and the electronic and vibrational energy highly contributes to the absorption and the translational and rotational energy highly contributes to the emissivity.
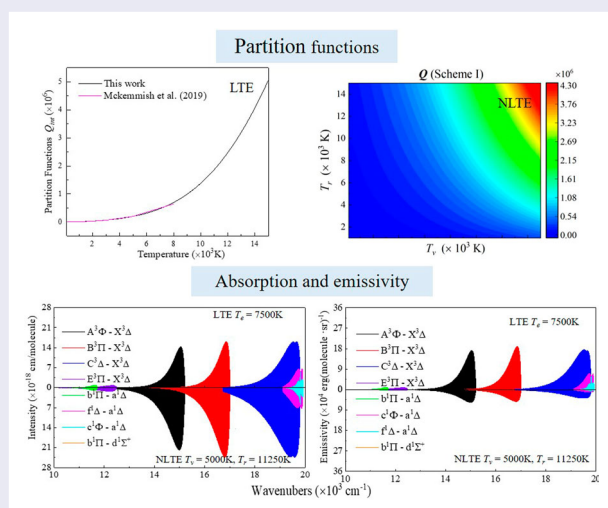
1. Introduction

Hypersonic vehicles need to fly through the denser atmosphere at an extremely high speed. A strong compression on the incident gas in front of the vehicle can heat the gas up to 10,000 K, leading to a strong heat transfer to the wall [1]. Under these conditions, the thermal protection system (TPS) is crucial to the design of vehicles, and the carbon/carbon (C/C) composites modified by

CONTACT Zhi Qin ✉ z.qin@sdu.edu.cn 🖅 Optics and Thermal Radiation Research Center, Institute of Frontier and Interdisciplinary Science, Shandong University, Qingdao, Shandong 266237, People's Republic of China; School of Information Science and Engineering, Shandong University, Qingdao, People's Republic of China; Linhua Liu ✉ liulinhua@sdu.edu.cn 🖅 School of Energy and Power Engineering, Shandong University, Jinan, Shandong 250061, People's Republic of China; Optics and Thermal Radiation Research Center, Institute of Frontier and Interdisciplinary Science, Shandong University, Qingdao, Shandong 266237, People's Republic of China; School of Energy Science and Engineering, Harbin Institute of Technology, Harbin, Heilongjiang 150001, People's Republic of China

Titanium (Ti) have been promising candidates due to their excellent properties such as low thermal expansion and good thermal resistance [2–4]. During hypersonic flights, TiO, as an intermediate product of the oxidation process, exists in the surrounding high-temperature shock layer [5]. Owing to the low characteristic time scales of the fluid with respect to equilibration time scales, the gas flow (including TiO) in the shock layer is in thermal and chemical nonequilibrium. To accurately predict aerodynamic heat loads on the TPS, the equilibrium and nonequilibrium thermodynamic and radiative characteristics of TiO at high temperatures are required.

As required in the study of the high-temperature flow of hypersonic vehicles, the internal partition functions (IPFs), average internal energies (AIEs) and internal specific heats (ISHs) in the LTE and NLTE for air and CO_2-N_2 plasma components, e.g. N_2, NO, O_2, CN, C_2, CO and CO^+, etc., have been calculated in the previous publication [6,7]. However, as for the important exotic molecule, TiO, only the partition functions in the LTE were calculated by Mckemmish et al. [8], Schwenke [9] and Tatum [10], where the results from Mckemmish et al. should be more credible because their PECs are obtained by fitting the experimental wavenumbers. Noted that the PECs from Mckemmish et al. only covered small internuclear distances around the equilibrium position so their IPFs were valid for temperatures up to 8000 K, which was lower than the temperature of the shock layer around the vehicle. Thus, the IPFs at higher temperatures are required to accurately estimate the heat flux in the shock layer. The other thermodynamic of TiO, such as the AIEs and ISHs in the LTE and NLTE, have not been investigated so far, which are essential for designing the thermal protection system. For the radiative properties, the absorption line intensities of TiO have been calculated at 296 K, and the $A^3\Phi-X^3\Delta$ transition at 1000 and 3000 K in the LTE were investigated as well [11,12], but other important transitions at higher temperatures and the transitions between different rotational energy levels were not considered in the calculations. In addition, the radiative properties of TiO in the NLTE have not been investigated so far, which are required to predict heat loads in thermal and chemical nonequilibrium. Therefore, a comprehensive study on a manifold of the thermodynamic and radiative properties for TiO is required.

The potential energy curves (PECs) are the basis for the calculation of IPFs of TiO, which are the starting point to derive thermodynamic and radiative data [13]. Many researches have been done to obtain accurate PECs experimentally [14–20]. However, theoretical calculations are limited and need to be investigated further. For example, although the PECs for 25 electronic states of TiO at the different levels of theory were calculated by Miliordos and Mavridis [21], the fitted spectroscopic constants for only several electronic states calculated by the internally contracted multireference configuration interaction (icMRCI) method were in good agreement with the experimental values [21]. Even so, Cheng et al. [11] recently investigated the PECs at the highly accurate MRCI level of theory with the Davidson correction (+Q) to obtain the spectroscopic data, whereas the spectroscopic constants were inconsistent with the experimental ones for some higher-lying states due to the small active space and basis sets adopted. Therefore, although TiO, as the first-row transition metal monoxide, has captured considerable attention in theory, there are still many challenges about how to accurately computing its PECs, which include spin contamination, symmetry breaking in the reference function, strong nondynamical electron correlation effects, etc. Meanwhile, TiO has many closely lying electronic states leading to interaction of even greater complexity, which needs including more core electrons into the active space [22].

In this work, we used the state-of-the-art *ab initio* methodology to investigate the thermodynamic and radiative properties of TiO, such as the IPFs, AIEs, ISHs, absorption line intensity and emissivity at temperatures from 100 to 15,000 K in the LTE and NLTE. As the basis for calculating the thermodynamic properties, the PECs of fifteen electronic states were calculated at the icMRCI + Q/aug-cc−pwCV5Z-DK level of theory. Based on our calculated PECs, the rovibrational energy levels for these fifteen states were determined by solving the nucleus Schrödinger equation and then used to compute the IPFs, AIEs and ISHs in the LTE and NLTE. The transition dipole moments (TDMs) and radiative lifetimes of eight transitions were also computed to obtain the absorption line intensity and emissivity of TiO in the LTE and NLTE.

2. Computational details

2.1. Potential energy curves and transition dipole moments

The PECs and TDMs of TiO were computed by the complete active space self-consistent field (CASSCF) method followed by the icMRCI + Q method over the internuclear range from 1.12 to 5.0 Å [23–25], which were carried out with MOLPRO 2015 program package [26]. The scanning step was 0.2 Å for each state, except the near equilibrium position where the point spacing was 0.02 Å. To obtain an accurate description of the PECs over a wide range of internuclear distance, a larger basis set, aug-cc-pwCV5Z-DK, was used.

All the calculations were carried out in C_{2v} group. The electrons in the 1s, 2s, 2p, 3s, 3p shell of Ti and 1s shell of O were put into ten closed-shell orbitals with six a_1 orbitals, two b_1 orbitals and two b_2 orbitals. The rest of electrons were put into the active spaces, which include six a_1 orbitals, one a_2 orbital, three b_1 orbitals and three b_2 orbitals, corresponding to 3d, 4s, 4p atomic orbitals of Ti and 2s, 2p orbitals of O [21].

According to the PECs, vibrational level energy (G_v) and inertial rotational constant (B_v) for the vibrational levels were obtained via numerically solving the one-dimensional Schrödinger equation of nuclear motion with the LEVEL 8.0 program package [27]. Thus, the spectroscopic constants can be determined at each vibrational quantum number v, and they can be expanded as

$$G_v = \sum_{l=0}^{n} Y_{l,0} \left(v + \frac{1}{2} \right)^l$$

$$= T_e + \omega_e \left(v + \frac{1}{2} \right) - \omega_e \chi_e \left(v + \frac{1}{2} \right)^2 + \cdots \quad (1)$$

$$B_v = \sum_{l=0}^{n} Y_{l,1} \left(v + \frac{1}{2} \right)^l = B_e - \alpha_e \left(v + \frac{1}{2} \right) + \cdots \quad (2)$$

where $Y_{l,0}$ and $Y_{l,1}$ are Dunham coefficients arranged by equilibrium spectroscopic constants that are adjusted on the vibration energy at each vibrational quantum number v. In general, the spectroscopic constants are fitted by five or six vibrational energy levels in the experiments. For example, the spectroscopic constants of the $X^3\Delta$ and $A^3\Phi$ states were fitted by the vibrational levels of $v = 0$, 1, 2, 3, 4 [20], and six vibrational levels were used to fit the spectroscopic constants of the $d^1\Sigma^+$ and $D^3\Delta$ states [28,29]. Therefore, six vibrational levels were used to determine the spectroscopic constants in this work.

The calculated PECs and TDMs can be used to obtain the Einstein coefficients of spontaneous emissions A_{fi}, which can be calculated by

$$A_{fi} = 2.026 \times 10^{-6} v_{fi}^3 \frac{2 - \delta_{0,\Lambda_i+\Lambda_f}}{2 - \delta_{0,\Lambda_i}}$$

$$\times \left[\int_0^\infty \psi_i(r) R_e(r) \psi_f(r) \right]^2 \quad (3)$$

where v_{fi} is the transition wavenumber and $\psi_i(r)$ and $\psi_f(r)$ are the vibrational wave functions of the initial and final electronic states, respectively.

2.2. Thermodynamic properties

2.2.1. Equilibrium thermodynamic properties
The population of rovibrational levels can be calculated using a Boltzmann distribution in the LTE. Thus, the IPFs

of TiO molecule were computed by

$$Q(T) = \sigma \sum_{n}^{n_{max}} (2 - \delta_{\Lambda,0})(2S + 1) \sum_{v}^{v_{max}(n)} \sum_{J}^{J_{max}(n,v)}$$

$$\times (2J + 1) \exp \left(-hc \frac{E_{n,v,J} - \varepsilon_0}{k_B T} \right) \quad (4)$$

where h, k_B and c are the Planck's constant, Boltzmann constant and the speed of light in vacuum, respectively. σ is the symmetry factor and sets to 1 for the heteronuclear molecule and S is the spin quantum number. $E_{n,v,J}$ is the energy of the n-th electronic state with quantum numbers Λ, v, J. ϵ_0 refers to the energy of the lowest energy level.

For 1 mole of TiO gas at the equilibrium temperature T, the AIEs (E_{int}) can be obtained from the first derivative of the IPFs

$$E_{int}(T) = RT^2 \left(\frac{\partial \ln Q(T)}{\partial T} \right) \quad (5)$$

and the ISHs (C_p) can be calculated from the second derivative

$$C_p(T) = \frac{\partial E_{int}(T)}{\partial T}$$

$$= R \left[2T \left(\frac{\partial \ln Q}{\partial T} \right) + T^2 \left(\frac{\partial^2 \ln Q}{\partial T^2} \right) \right] \quad (6)$$

where R is the gas constant. The detailed descriptions on the calculations of the IPFs, AIEs and ISHs can refer to our previous work [6].

2.2.2. Non-equilibrium thermodynamic properties
The two-temperature model is the primary choice to deal with the IPFs in the NLTE. Based on the rovibrational energy partitioning scheme proposed by Jaffe [30], the two-temperature IPFs of TiO corresponding to two limiting cases, denoted by Schemes I and II, were calculated by

$$Q^I(T_v, T_r) = \sigma \sum_{n=0}^{n_{max}} (2 - \delta_{\Lambda,0})(2S + 1) e^{-\frac{E_{n,0,0}}{RT_v}} \sum_{v=0}^{v_{max}(n)}$$

$$\times e^{-\frac{E_{n,v,0} - \varepsilon_0}{RT_v}} \sum_{J=0}^{J_{max}(n,v)} (2J + 1) e^{-\frac{\Delta^I E(n,v,J) - \varepsilon_0}{RT_r}}$$

$$(7)$$

$$Q^{II}(T_v, T_r) = \sigma \sum_{n=0}^{n_{max}} (2 - \delta_{\Lambda,0})(2S + 1) e^{-\frac{E_{n,0,0}}{RT_r}} \sum_{J=0}^{J_{max}(n)}$$

$$\times (2J + 1) e^{-\frac{E_{n,0,J} - \varepsilon_0}{RT_r}} \sum_{v=0}^{v_{max}(n,J)} e^{-\frac{\Delta^{II} E(n,v,J) - \varepsilon_0}{RT_v}}$$

$$(8)$$

where T_r is the temperature of the rotational and translational energy levels and T_v is the temperature of the electronic and vibrational energy levels. R is the gas constant, $R = k_B/hc$. $\Delta^I E\,(n, v, J)$ and $\Delta^{II} E\,(n, v, J)$ were obtained by

$$\Delta^I E(n, v, J) = E_{n,0,J} + E_{\text{inter}}(n, v, J) \tag{9}$$

$$\Delta^{II} E(n, v, J) = E_{n,v,0} + E_{\text{inter}}(n, v, J) \tag{10}$$

where $E_{\text{inter}}\,(n, v, J)$ is the interaction energy, describing that the rotational energy levels are perturbed by vibration or that the vibrational energy levels are perturbed by rotation, $E_{\text{inter}}\,(n, v, J) = E_{n,v,J} - E_{n,v,0} - E_{n,0,J} + E_{n,0,0}$ [30]. Then, the two-temperature AIEs (E_{int}) can be derived as

$$E_{\text{int}}^I(T_v, T_r) = RT_v^2 \frac{\partial \ln Q^I(T_v, T_r)}{\partial T_v} \tag{11}$$

$$E_{\text{int}}^{II}(T_v, T_r) = RT_r^2 \frac{\partial \ln Q^{II}(T_v, T_r)}{\partial T_r} \tag{12}$$

and the dimensional AIEs were computed by

$$\overline{E_{\text{int}}} = \frac{E_{\text{int}}(T_v, T_r)}{R\sqrt{T_v, T_r}} \tag{13}$$

Thus the vibrational and rotational ISHs were obtained by the numerical difference method

$$C_{p,\text{vib}}(T_v, T_r) = \frac{\partial E_{\text{int}}^I(T_v, T_r)}{\partial T_v} \tag{14}$$

$$C_{p,rot}(T_v, T_r) = \frac{\partial E_{int}^{II}(T_v, T_r)}{\partial T_r} \tag{15}$$

The dimensional vibrational and rotational ISHs were calculated by

$$\overline{C_p}(T_v, T_r) = \frac{C_p(T_v, T_r)}{R} \tag{16}$$

2.3. Radiative properties

2.3.1. Equilibrium radiative properties

The absorption line intensity I_{fi} (cm molecule^{-1}) of TiO in the LTE can be given [31]

$$I(f \leftarrow i) = \frac{g_f^{tot} A_{fi}}{8\pi c v_{fi}^2} \frac{e^{-\frac{E_i}{RT}}\left(1 - e^{-\frac{v_{fi}}{RT}}\right)}{Q(T)} \tag{17}$$

where A_{fi} is the Einstein-A coefficient (s^{-1}), g_f^{tot} is the total degeneracy, and the units of the energy E and temperature T are cm^{-1} and K, respectively. The emissivity (erg (molecule $\cdot$ sr)$^{-1}$) can be calculated by

$$\varepsilon(i \rightarrow f) = \frac{g_i^{tot} A_{fi} v_{fi}}{4\pi} \frac{e^{-\frac{E_i}{RT}}}{Q(T)} \tag{18}$$

2.3.2. Non-equilibrium radiative properties

For the radiative properties of TiO in the NLTE, the two-temperature model is used to describe the rovibrational energy partitioning. For example, the emissivity under the two partitioning schemes can be calculated by

$$\varepsilon_{if}^I(T_v, T_r) = \frac{g_i^{tot} A_{fi} v_{fi}}{4\pi Q(T)} e^{-\frac{E_{i,0,0}}{RT_v}} e^{-\frac{E_{i,v_i,0} - \varepsilon_0}{RT_v}} e^{-\frac{\Delta^I E(i,v_i,J_i) - \varepsilon_0}{RT_r}} \tag{19}$$

$$\varepsilon_{if}^{II}(T_v, T_r) = \frac{g_i^{tot} A_{fi} v_{fi}}{4\pi Q(T)} e^{-\frac{E_{i,0,0}}{RT_r}} e^{-\frac{E_{i,0,J_i} - \varepsilon_0}{RT_r}} e^{-\frac{\Delta^{II} E(i,v_i,J_i) - \varepsilon_0}{RT_v}} \tag{20}$$

3. Results and discussion

3.1. Potential energy curves and transition dipole moments

3.1.1. Potential energy curves

Seven triplets (X$^3\Delta$, E$^3\Pi$, D$^3\Sigma^-$, A$^3\Phi$, B$^3\Pi$, C$^3\Delta$ and F$^3\Sigma^+$) and eight singlet states (a$^1\Delta$, d$^1\Sigma^+$, b$^1\Pi$, 1$^1\Gamma$, h$^1\Sigma^+$, 2$^1\Pi$, c$^1\Phi$ and f$^1\Delta$) were investigated in this work. Figure 1 displays the calculated PECs of these states. All of these electronic states correlate to the lowest dissociation asymptote, Ti (^{3}F) + O (^{3}P). Obviously, there are many crossings of different symmetries. The corresponding spectroscopic constants, including the adiabatic excitation energy (T_e), equilibrium internuclear distance (R_e), vibrational constant (ω_e and $\omega_e \chi_e$), rotational constant (B_e), and ro-vibrational coupling constant (α_e), were determined by six vibrational levels (from $v = 0$ to $v = 5$) and listed in Table 1, where the vibrational and rotational constants associated with the energy level are very important to the further calculations of the IPFs. Experimentally, except for the F$^3\Sigma^+$, 1$^1\Gamma$, h$^1\Sigma^+$ and 2$^1\Pi$ states, all the other states have been detected. The calculated spectroscopic constants of these states in our work are more consistent with the earlier experimental results than those from Cheng et al. [11], this owes to the core-valence correlation considered in our calculations. Especially, for the X$^3\Delta$, A$^3\Phi$, B$^3\Pi$, a$^1\Delta$, d$^1\Sigma^+$, c$^1\Phi$, and f$^1\Delta$ states, the spectroscopic constants ω_e differ from the experimental ones by only less than 10 cm^{-1}. In addition, our calculated ω_e of the E$^3\Pi$ and C$^3\Delta$ states differ by less than 15 cm^{-1}. For the b$^1\Pi$ and D$^3\Sigma^-$ states, the calculated ω_e does not reproduce the experimental value well, but the value of the D$^3\Sigma^-$ state is closer to the theoretical result from Miliordos and Mavridis [21]. For the undetected F$^3\Sigma^+$, 1$^1\Gamma$, h$^1\Sigma^+$ and 2$^1\Pi$ electronic states, our spectroscopic constants are also in good agreement with the theoretical values [21].
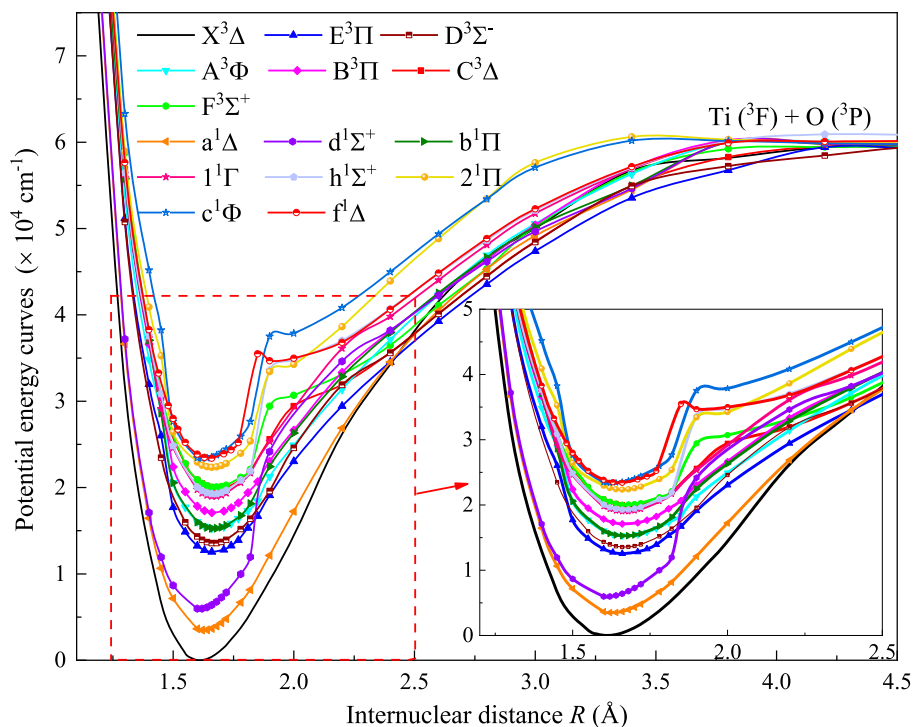
Figure 1. The PECs of fifteen electronic states of TiO at the icMRCI + Q/aug-cc- pwCV5Z-DK level of theory.

3.1.2. Transition dipole moments and radiative lifetimes

Eight transitions, including four transitions between singlets and four transitions between triplets, were investigated, and the TDMs for these transitions are displayed in Figure 2. Using the calculated PECs and TDMs, the radiative lifetimes of six electronic states, including the $A^3\Phi$, $B^3\Pi$, $C^3\Delta$, $b^1\Pi$, $c^1\Phi$ and $f^1\Delta$ states, can be obtained and listed in Table 2. Except the $b^1\Pi$ state, the radiative lifetimes of the other five states have been measured experimentally by Hedgecock et al. [35]. Our calculated radiative lifetimes of the $A^3\Phi$, $B^3\Pi$ and $C^3\Delta$ states are close to the experimental results. Due to the larger TDMs for the $C^3\Delta$ - $X^3\Delta$ transition near the equilibrium internuclear distance, the radiative lifetimes of the $C^3\Delta$ are shorter. For the $c^1\Phi$ and $f^1\Delta$ states, only the radiative lifetimes of the vibrational level $v = 0$ were detected, and there is a slight difference with our results. Compared with the previous theoretical results, our calculated radiative lifetimes of the $b^1\Pi$ state are shorter than the results from Schamps et al. [36] but longer than those from Cheng et al. and Langhoff et al. [11,37], because of the smaller TDMs near the equilibrium internuclear distance in this work than those in the calculations of Cheng et al. [11]. The vibrational radiative lifetimes of the $A^3\Phi$, $B^3\Pi$, $b^1\Pi$ and $f^1\Delta$ states increase for $v' > 6$. According to the wave-mechanical formulation of the Franck-Condon principle, the transitions from the vibrational level $v' = 6$ has a maximum value of the overlap

integral of the wavefunctions and thus the radiative lifetimes of upper states are shorter at $v' = 6$. Besides, due to the similar equilibrium distances of the upper and lower electronic states, the trends of the radiative lifetimes of the upper states via the $A^3\Phi$-$X^3\Delta$, $B^3\Pi$-$X^3\Delta$, $b^1\Pi$-$a^1\Delta$, $b^1\Pi$-$d^1\Sigma^+$ and $f^1\Delta$-$a^1\Delta$ transitions are similar. For example, the equilibrium distances of the lower states, $X^3\Delta$, $a^1\Delta$ and $d^1\Sigma^+$, are about 1.61–1.62 Å, and the equilibrium distances of the $A^3\Phi$, $B^3\Pi$, $b^1\Pi$ and $f^1\Delta$ states are about 1.70 Å. However, the equilibrium distances of the $C^3\Delta$ and $c^1\Phi$ states are 1.687 and 1.623Å, respectively, which leads to the different vibrational levels with a short radiative lifetime. For example, the vibrational levels of the $C^3\Delta$ and $c^1\Phi$ states with the short radiative lifetime are $v' = 4$ and $v' = 0$, respectively.

3.2. Thermodynamic properties

3.2.1. Thermodynamic properties in the local thermal equilibrium

The thermodynamic properties, including the IPFs (Q_{int}), AIEs (E_{int}) and ISHs (C_p), of TiO in the LTE over the temperatures from 100 to 15,000 K were calculated. In order to analyse the effect of different numbers of electronic states on the IPFs, Figure 3(a,b) shows the IPFs and dimensional ISHs (C_p/R) calculated by different numbers of electronic states and a comparison of the IPFs with those from Mckemmish et al. [8], where n is the number of the electronic state considered in the calculation of the

Table 1. Spectroscopic constants of fifteen states of TiO obtained by the icMRCI + Q/aug-cc-pwCV5Z-DK method.

State		T_e/cm⁻¹	ω_e/cm⁻¹	$\omega_e x_e$	B_e	$\alpha_e/\times10^{-3}$cm⁻¹	r_e/Å
$X^3\Delta$	This work	0	1018.83	7.4649	0.5416	5.27	1.613
	Exp. [20]	0	1009.18	4.5617	0.5353	3.0237	1.6203
	Cal. [21]	0	1010	5.4	–	2.9	1.623
	Cal. [11]	0	1008.99	4.61	0.53		1.612
$a^1\Delta$	This work	3497.52	1015.73	9.0711	0.5318	4.88	1.629
	Exp. [32]		1018.27	4.521	0.5376	2.916	1.617
	Exp. [18]	3443.28					
	Cal. [21]	3771	1017	4.7		2.4	1.621
	Cal. [11]	3083.61	1095.14	8.57	0.54		1.609
$d^1\Sigma^+$	This work	5974.89	1014.57	4.6134	0.5428	3.25	1.609
	Exp. [28]		1023.06	4.8935	0.5493	3.3483	
	Exp. [15]	5663.15					
	Cal. [21]	7546	1016	4.2		3.5	1.603
	Cal. [11]	5305.65	1118.46	7.45	0.56		1.594
$E^3\Pi$	This work	12,543.74	900.80	8.4634	0.5074	6.31	1.677
	Exp. [19]	11,870.2	912.90	5.1	0.5167	3.235	1.6493
	Cal. [21]	12,359	896	5.2		3.1	1.673
	Cal. [11]	11,345.35	1038.35	8.38	0.52		1.640
$D^3\Sigma^-$	This work	13,556.80	927.32	6.1187	0.5053	2.43	1.681
	Expt. [33]	12,284	968	5.369	0.5105	3.62174	1.659
	Cal. [21]	13,256	893	4.6		2.6	1.682
	Cal. [11]	12,638.35	1137.70	34.51	0.51		1.651
$b^1\Pi$	This work	15,276.84	874.24	4.5097	0.5055	4.77	1.668
	Exp. [28]		919.76	4.2791	0.5135	2.839	
	Exp. [29]						1.6546
	Exp. [15]	14,717.19					
	Cal. [21]	15,278	891	4.0		2.5	1.677
	Cal. [11]	14,200.15	1005.56	9.28	0.51		1.638
$A^3\Phi$	This work	15,289.41	868.71	10.10	0.5051	7.39	1.672
	Exp. [20]		867.52	3.833	0.5073	3.1666	1.6645
	Exp. [33]	14,094.17					
	Cal. [21]	14,417	822	2.6		2.9	1.684
	Cal. [11]	13,947.45	921.76	23.23	0.50		1.669
$B^3\Pi$	This work	17,089.41	856.93	11.7804	0.5039	4.71	1.672
	Exp. [34]	16,219.18	865.88	0.9246	0.5076	3.179	1.664
	Cal. [21]	16,579	833	2.9		3.1	1.682
	Cal. [11]	16,173.24	979.98	15.18	0.51		1.654
$1^1\Gamma$	This work	18,981.79	912.79	1.7406	0.5047	1.99	1.668
	Cal. [21]	17,953	913	3.3		3.0	1.670
	Cal. [11]	15,385.96	1001.75	6.20	0.52		1.638
$h^1\Sigma^+$	This work	19274.66	966.8	41.8973	0.5108	12.36	1.668
	Cal. [9]	17,564.88	852.12	5.61	0.4881	5.46	
	Cal. [21]	18,596	913	4.6		3.1	1.669
	Cal. [11]	17,750.62	1025.91	6.74	0.52		1.634
$C^3\Delta$	This work	19,856.05	853.90	4.2711	0.4933	0.54	1.687
	Exp. [29]	19,424.87	838.26	4.7592	0.4899	3.062	1.6938
	Cal. [21]	18,927	813	1.3		3.5	1.712
	Cal. [11]	18,951.57	995.63	39.87	0.49		1.680
$F^3\Sigma^+$	This work	20,028.11	849.83	7.0817	0.5041	12.62	1.663
	Cal. [21]	19,825	840	7.9		3.3	1.719
$2^1\Pi$	This work	22,343.66	882.27	6.0364	0.5097	5.50	1.661
	Cal. [21]	21100	924	4.0		3.4	1.644
$c^1\Phi$	This work	23,374.73	923.86	6.9469	0.5335	11.32	1.623
	Exp. [18]	21,278.90			0.5230	3.411	1.6393
	Exp. [29]		917.55	4.42			
	Cal. [21]	21,614	938	4.5		4.1	1.644
	Cal. [11]	20,788.29	1207.81	37.21	0.52		1.625
$f^1\Delta$	This work	23,392.90	883.70	26.3996	0.5168	8.60	1.655
	Exp. [15]	22,513.36					
	Exp. [32]		874.10	2.5		3.08	1.6701
	Cal. [21]	22,353	870	3.4		3.0	1.680
	Cal. [11]	29,212.55	789.14	34.18	0.50		1.668

IPFs and ISHs. Our IPFs are consistent with the previous results from Mckemmish et al. [8] at the low temperatures (< 8000 K), who considered sixteen electronic states and used the analytical spectroscopic model from theoretical and experimental data. Based on the calculated IPFs, the ISHs can be obtained. The dimensional ISHs start from the value of 1 because of the activation of the rotational degrees of freedom and then rapidly reach the value of 2, which includes the vibrational contribution from the ground electronic state. The similar phenomenon can be
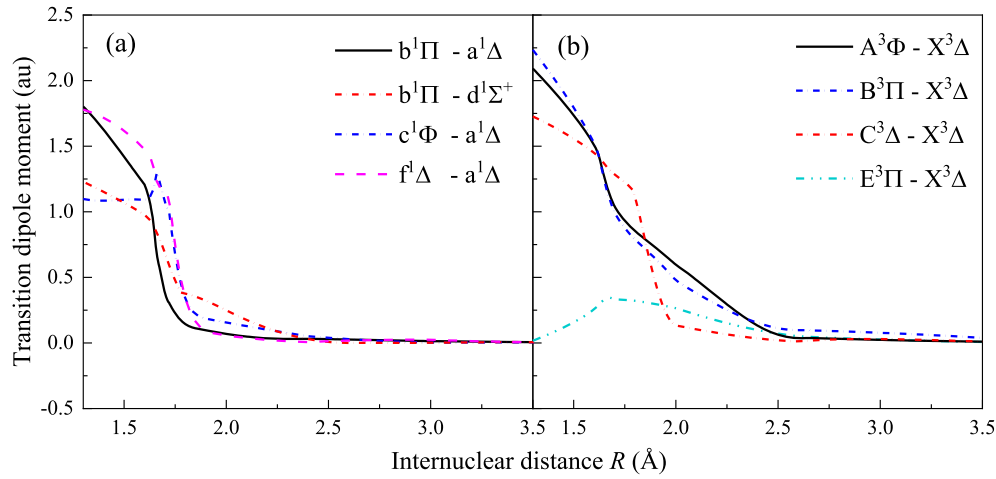
Figure 2. The TDMs of eight transitions between singlet and triplet states of TiO.

Table 2. Vibrational radiative lifetimes of the $A^3\Phi$ state via the $A^3\Phi$-$X^3\Delta$ transition, of the $B^3\Pi$ state via the $B^3\Pi$-$X^3\Delta$ transition, of the $C^3\Delta$ state via the $C^3\Delta$-$X^3\Delta$ transition, of the $E^3\Pi$ state via the $E^3\Pi$-$X^3\Delta$ transition, of the $b^1\Pi$ state via the $b^1\Pi$-$a^1\Delta$ and $b^1\Pi$-$d^1\Sigma^+$ transitions, of the $c^1\Phi$ state via the $c^1\Phi$-$a^1\Delta$ transition, and of the $f^1\Delta$ state via the $f^1\Delta$-$a^1\Delta$ transition.

| v'		0	1	2	3	4	5	6	7	8
$A^3\Phi$	This work	109.57	96.78	93.03	89.62	83.80	79.96	79.20	81.29	85.41
	Exp. [35]	103.3±3.6	112.9±1.8							
	Exp. [38]	102.4±3.5								
	Cal. [37]	96.6	95.8							
	Cal. [36]	55.2								
	Cal. [11]	104.1	107.4	102.5	115.2	95.5	108.1	105.6		
$B^3\Pi$	This work	60.60	69.12	63.92	61.14	59.55	57.90	57.66	59.68	62.65
	Exp. [35]	65.6±1.2	66.5±1.0	63.8±1.4						
	Exp. [38]	54.4±3.6								
	Cal. [37]	60.7	60.1	60.0						
	Cal. [36]	56.2								
	Cal. [11]	67.4	64.7	61.3	68.2	58.1	65.5	59.5		
$C^3\Delta$	This work	41.94	40.92	39.51	39.01	38.65	39.54	40.14	42.68	45.21
	Exp. [35]	43.3±1.0	43.0±1.2							
	Exp. [38]			18.5±3						
	Cal. [36]	38.7								
	Cal. [11]	41.2	39.7	36.5	34.6	37.7	22.8	21.3		
$b^1\Pi$	This work	286.33	228.35	206.42	191.16	185.65	182.89	179.50	181.91	193.11
	Cal. [37]	119.7	121.0							
	Cal. [36]	455								
	Cal. [11]	108.1	116.7	105.5	93.1	87.8	85.1	78.8		
$c^1\Phi$	This work	46.13	52.34	64.19	75.24	73.45	74.18	71.80	71.23	72.17
	Exp. [35]	38.3±1.6								
	Cal. [37]	27.5	28.1							
	Cal. [36]	15								
	Cal. [11]	34.9	40.0	52.3	42.5	43.1	45.0	49.1		
$f^1\Delta$	This work	34.34	34.05	32.29	31.02	30.31	29.74	29.71	30.36	31.89
	Exp. [35]	43.2±2.0								
	Cal. [37]	37.6	37.3							
	Cal. [36]	41.6								
	Cal. [11]	42.9	35.4	44.5	43.4	43.5	42.8	62.5		

seen in other diatomic molecules, such as CN, C_2, and CO [6].

To investigate the contributions of different electronic states to the total IPFs, the proportion of a specific electronic state to the total IPFs was calculated. For example,

the proportion of the $E^3\Pi$ state was computed by

$$w_{E^3\Pi}(T) = \frac{Q_{X^3\Delta+a^1\Delta+d^1\Sigma^++E^3\Pi}(T) - Q_{X^3\Delta+a^1\Delta+d^1\Sigma^+}(T)}{Q_{\text{total}}(T)} \quad (21)$$
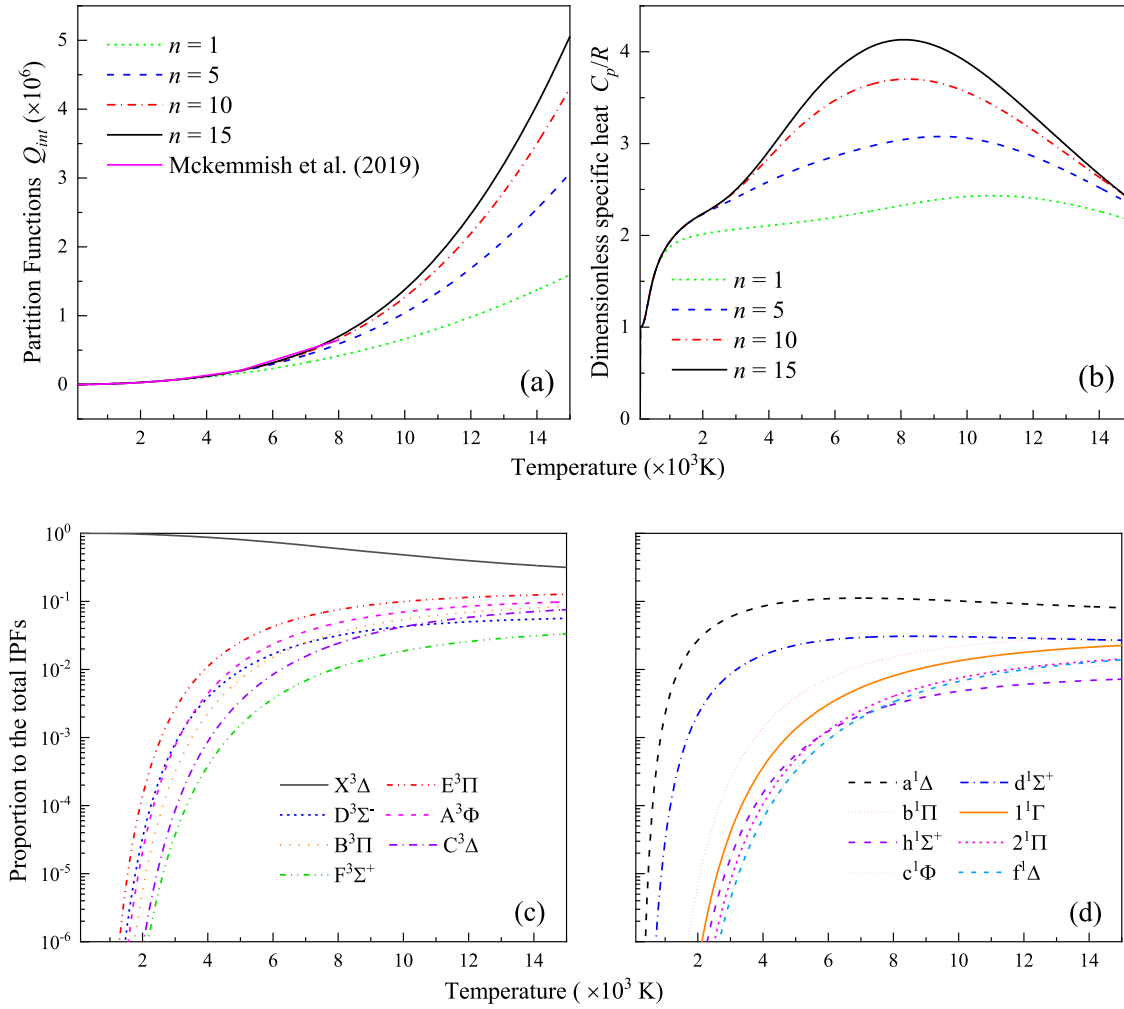
Figure 3. Curves of (a) the IPFs and (b) the ISHs calculated by n (n = 1, 5, 10, 15) electronic states, and the proportions of (a) triplet and (b) singlet electronic states to the total IPFs. Note that n = 1 denotes the results obtained only by the ground state, n = 5 denotes the results calculated by the ground state and the success 4 excited states, n = 10 denotes the results calculated by the ground state and the success 9 excited states and n = 15 denotes the results calculated by all the calculated states.

where $Q_{X^3\Delta+a^1\Delta+d^1\Sigma^++E^3\Pi}$ (T) is the IPFs calculated by the $X^3\Delta$, $a^1\Delta$, $d^1\Sigma^+$ and $E^3\Pi$ states, Q_{total} (T) is the total IPFs calculated by fifteen states. The sum of the proportions of all states at a specific temperature is 1 and the proportions of different states are shown in Figure 3(c,d). To verify our results, Table 3 shows the calculated populations of the $X^3\Delta$, $D^3\Sigma^-$, $h^1\Sigma^+$ and $f^1\Delta$ states relative to total population at different temperatures and those from Mckemmish et al. [8]. Our calculated proportions are close to the previous theoretical results. For the low temperatures (< 860 K), the proportions of the ground state are about 1, thus the total IPFs are dominated by the $X^3\Delta$ state. As the temperature increases, the contributions of the ground state gradually decrease due to the increasing population density of excited states. For example, the proportions of the $a^1\Delta$ state and $d^1\Sigma^+$ states increase to 0.001 at 87 and 1700 K, respectively, which imply that they begin to take effect on the total IPFs.

According to the above analysis, we can conclude that one ($X^3\Delta$) and two ($X^3\Delta$ and $a^1\Delta$) states 'saturate' the IPFs at the temperature below 860 and 1700 K, respectively. Therefore, the electronic states that saturate the total IPFs at different temperature ranges can be summarised in Table 4.

3.2.2. Thermodynamic properties in the local thermal non-equilibrium

The two-temperature IPFs and AIEs versus vibrational and rotational temperatures (T_v and T_r) in the NLTE were calculated by considering fifteen electronic states from 100 to 15,000 K and displayed in Figure 4(a–d). A slight difference exists between the IPFs of the two energy partitioning schemes generally due to the negative effect of the interaction energy (E_{inter}), which also makes a difference between the AIEs. For example, the AIEs of the Scheme I for high T_v and low T_r are

Table 3. Population of different states relative to total population at different temperatures.

	1000K		3000K		5000K		8000K	
States	This work	Cal. [8]	This work	Cal. [8]	This work	Cal. [8]	This work	Cal. [8]
$X^3\Delta$	9.97×10^{-1}	9.97×10^{-1}	9.27×10^{-1}	9.21×10^{-1}	8.10×10^{-1}	7.91×10^{-1}	5.97×10^{-1}	5.76×10^{-1}
$D^3\Sigma^-$	2.02×10^{-9}	1.26×10^{-8}	8.13×10^{-4}	8.03×10^{-5}	9.56×10^{-3}	1.43×10^{-3}	3.15×10^{-2}	3.51×10^{-2}
$h^1\Sigma^+$	1.76×10^{-13}	1.96×10^{-12}	1.68×10^{-5}	3.78×10^{-5}	5.58×10^{-4}	9.58×10^{-4}	3.07×10^{-3}	4.68×10^{-3}
$f^1\Delta$	9.52×10^{-15}	3.70×10^{-15}	4.16×10^{-6}	7.82×10^{-6}	3.23×10^{-4}	4.98×10^{-4}	3.33×10^{-3}	4.03×10^{-3}

Table 4. The temperature ranges (K) corresponding to the electronic states that saturate the total IPFs.

Temperature ranges	Electronic states	Temperature ranges	Electronic states
100–870	$X^3\Delta$	3760–4090	$X^3\Delta, a^1\Delta, d^1\Sigma^+, E^3\Pi, D^3\Sigma^-, A^3\Phi, B^3\Pi, b^1\Pi$
870–1700	$X^3\Delta, a^1\Delta$	4090–4650	$X^3\Delta, a^1\Delta, d^1\Sigma^+, E^3\Pi, D^3\Sigma^-, A^3\Phi, B^3\Pi, b^1\Pi, C^3\Delta$
1700 - 2580	$X^3\Delta, a^1\Delta, d^1\Sigma^+$	4650 - 4730	$X^3\Delta, a^1\Delta, d^1\Sigma^+, E^3\Pi, D^3\Sigma^-, A^3\Phi, B^3\Pi, b^1\Pi, C^3\Delta, F^3\Sigma^+$
2580–3110	$X^3\Delta, a^1\Delta, d^1\Sigma^+, E^3\Pi$	4730–5690	$X^3\Delta, a^1\Delta, d^1\Sigma^+, E^3\Pi, D^3\Sigma^-, A^3\Phi, B^3\Pi, b^1\Pi, C^3\Delta, F^3\Sigma^+, 1^1\Gamma$
3110–3130	$X^3\Delta, a^1\Delta, d^1\Sigma^+, E^3\Pi, D^3\Sigma^-$	5690–5710	$X^3\Delta, a^1\Delta, d^1\Sigma^+, E^3\Pi, D^3\Sigma^-, A^3\Phi, B^3\Pi, b^1\Pi, C^3\Delta, F^3\Sigma^+, 1^1\Gamma, h^1\Sigma^+$
3130–3520	$X^3\Delta, a^1\Delta, d^1\Sigma^+, E^3\Pi, D^3\Sigma^-, A^3\Phi$	5710–6080	$X^3\Delta, a^1\Delta, d^1\Sigma^+, E^3\Pi, D^3\Sigma^-, A^3\Phi, B^3\Pi, b^1\Pi, C^3\Delta, F^3\Sigma^+, 1^1\Gamma, h^1\Sigma^+, 2^1\Pi$
3520–3760	$X^3\Delta, a^1\Delta, d^1\Sigma^+, E^3\Pi, D^3\Sigma^-, A^3\Phi, B^3\Pi$	6080–6090	$X^3\Delta, a^1\Delta, d^1\Sigma^+, E^3\Pi, D^3\Sigma^-, A^3\Phi, B^3\Pi, b^1\Pi, C^3\Delta, F^3\Sigma^+, 1^1\Gamma, h^1\Sigma^+, 2^1\Pi, c^1\Phi$

larger than those calculated by the Scheme II. This phenomenon is explained by Babou et al. [39] due to the higher electronic and vibrational energy contributions than the rotational ones. Based on the calculated AIEs, the vibrational and rotational ISHs by the two energy partitioning schemes were computed and shown in Figure 4 (e–h). Unlike the IPFs and AIEs, the vibrational and rotational ISHs ($C_{p,\text{vib}}$ or $C_{p,\text{rot}}$) are strongly affected by the energy partitioning schemes and depend more on the vibrational (rotational) temperature. Due to the higher electronic and vibrational energy contributions, the vibrational ISHs in the Scheme I are larger than other ISHs.

To investigate the effect of different numbers of electronic states on the IPFs, the IPFs versus vibrational (rotational) temperatures were calculated by the Scheme I (Scheme II) at T_r (T_v) = 7500 K and compared with the IPFs in the LTE, as shown in Figure 5. For the calculation of the same electronic states, the curves of the IPFs in the NLTE and the LTE intersect at 7500 K, which is reliable because the Equations (7) and (8) are the same as the Eq. (4) at $T_v = T_r$. In addition, the IPFs in the NLTE calculated by the two schemes are close in Figure 5(a) but differ from those in the LTE in Figure 5(b). At the temperatures below the intersection, the IPFs in the NLTE are larger than those in the LTE but this situation is opposite at high temperatures, this is because the higher equivalent temperature $T_e = (T_v\, T_r)^{0.5}$ in the NLTE causes the larger IPFs.

The proportions of different electronic states to the total population in the NLTE were also investigated, where the proportions by the Scheme I (Scheme II) as a function of the vibrational (rotational) temperature

were calculated at T_r (T_v) = 7500 K. For the sake of visual clarity, the proportions of only six electronic states were displayed in Figure 5(c). The proportions of a specific state in the NLTE are almost identical to those in the LTE, which reveal the condition of the gas (LTE or NLTE) may not affect the proportions. Therefore, the electronic states that saturate the IPFs at different temperature ranges in Table 3 can also be applied to the gas in the NLTE.

3.3. Radiative properties

3.3.1. Radiative properties in the local thermal equilibrium

The radiative properties of TiO in the high-temperature gases play a key role in the radiative transfer calculations to predict aerodynamic heat loads on the TPS, where the absorption line intensity and emissivity are the main parameters. Considering eight transitions and five vibrational levels of each electronic state, the absorption line intensity and emissivity in the LTE at the temperature of 7500 K are calculated and shown in Figure 6. The $A^3\Phi-X^3\Delta$, $B^3\Pi-X^3\Delta$ and $C^3\Delta-X^3\Delta$ transitions have the strong absorption and emissivity, where the 0–0 band of the $C^3\Delta-X^3\Delta$ system has the strongest excitation at 19,653cm^{-1} that is close to the wavelength of 517 nm calculated by Cheng et al. [11]. Experimentally, the 2–0 band of the $C^3\Delta-X^3\Delta$ transition has been detected and the wavelength is 476 nm, which is also consistent with our results (469.48 nm) [40]. As for the transitions between singlets, the intensities of the $f^1\Delta-a^1\Delta$ and $c^1\Phi-a^1\Delta$ transitions are also strong because of the short radiative lifetimes.
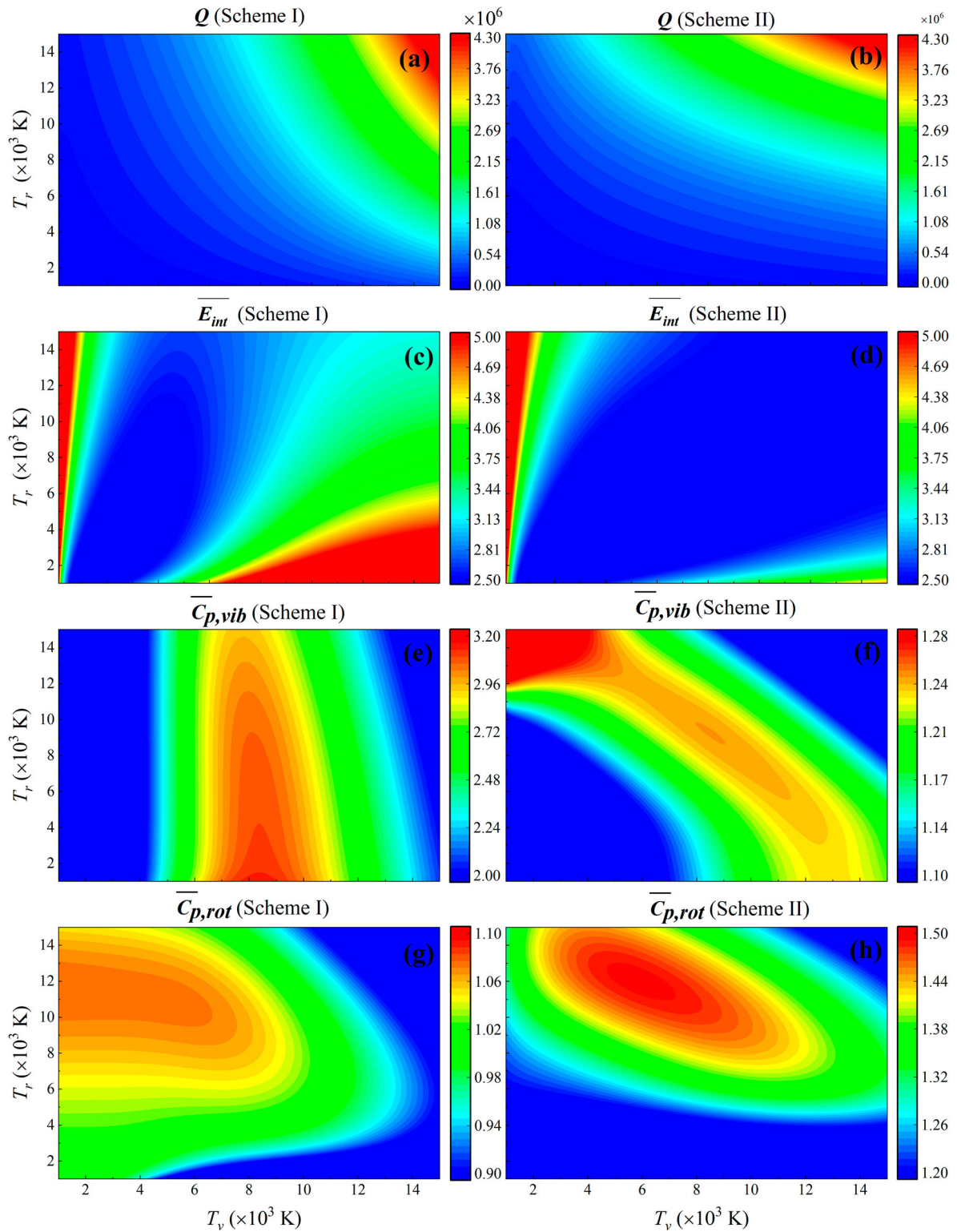
Figure 4. Contours of (a-b) the IPFs, (c-d) dimensionless AIEs, (e-f) dimensionless vibrational specific heat and (g-h) the dimensionless rotational specific heat for TiO versus vibrational (T_v) and rotational (T_r) temperatures according to the two energy partitioning schemes.
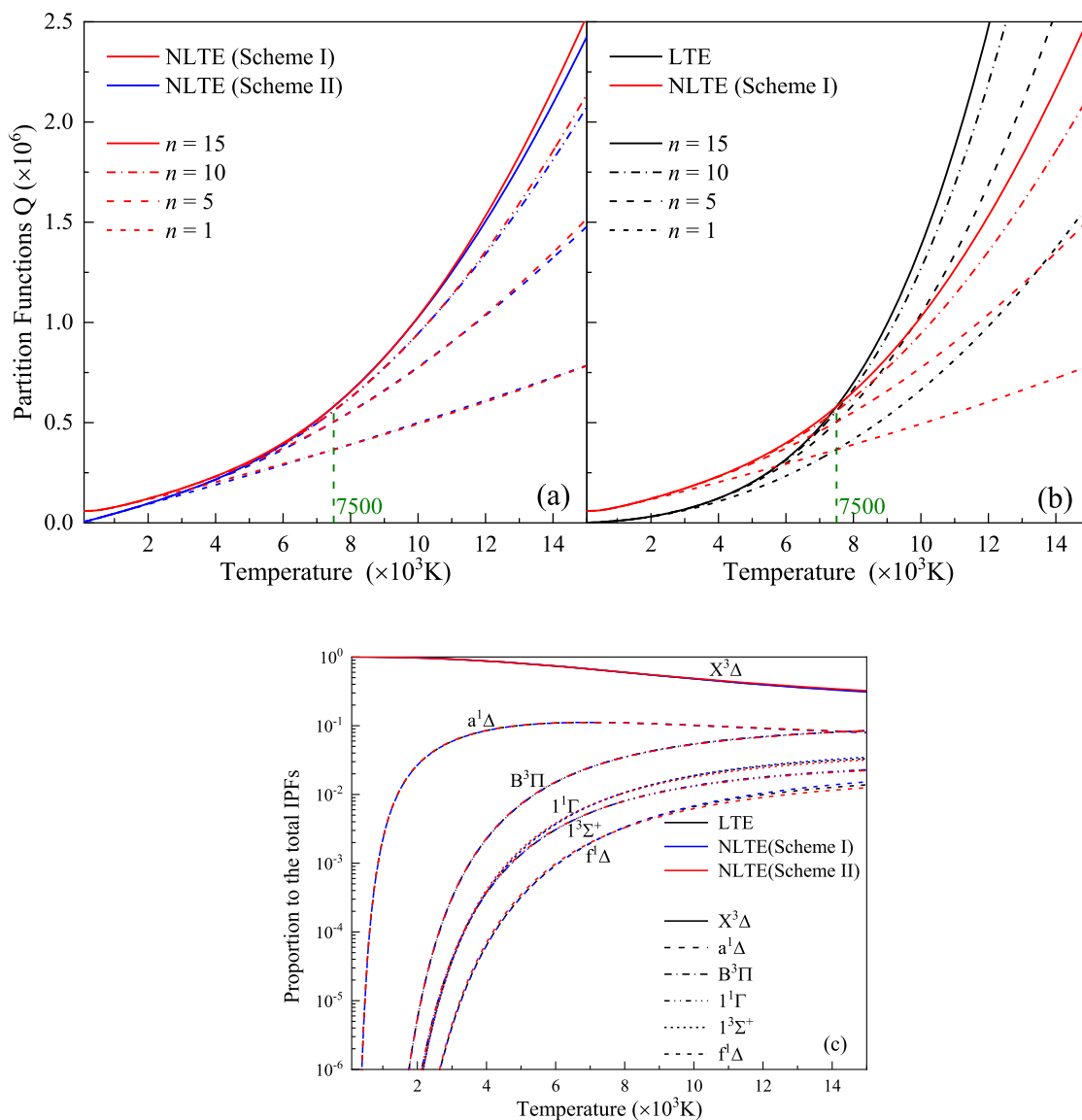
Figure 5. Curves of (a) the IPFs in the NLTE by the Scheme I (Scheme II) at T_r (T_v) = 7500 K considering n (n = 1, 5, 10, 15) electronic states, (b) a comparison of the IPFs in the NLTE with those in the LTE and (c) the proportion of a specific electronic state to the total IPFs.
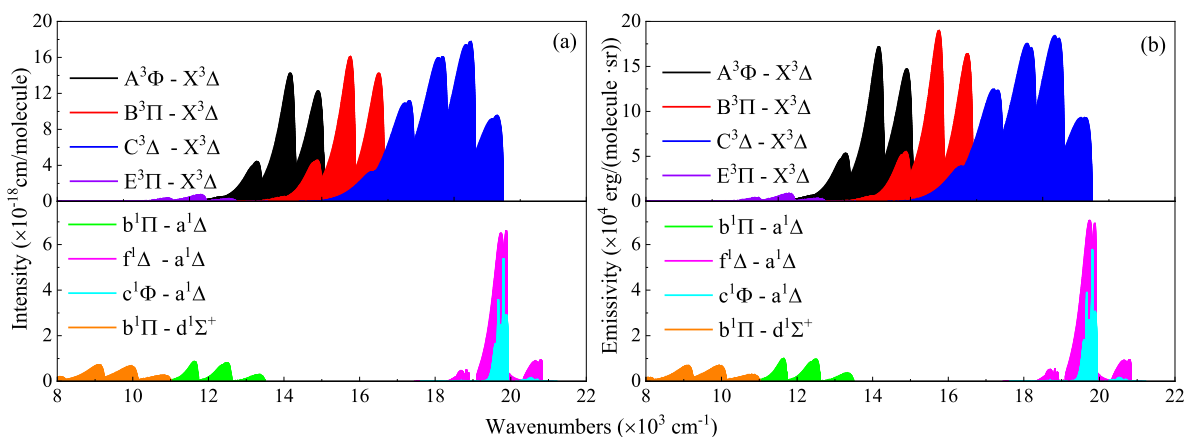
Figure 6. Radiative properties TiO at the temperature of 7500K: (a) absorption line intensity, (b) emissivity.
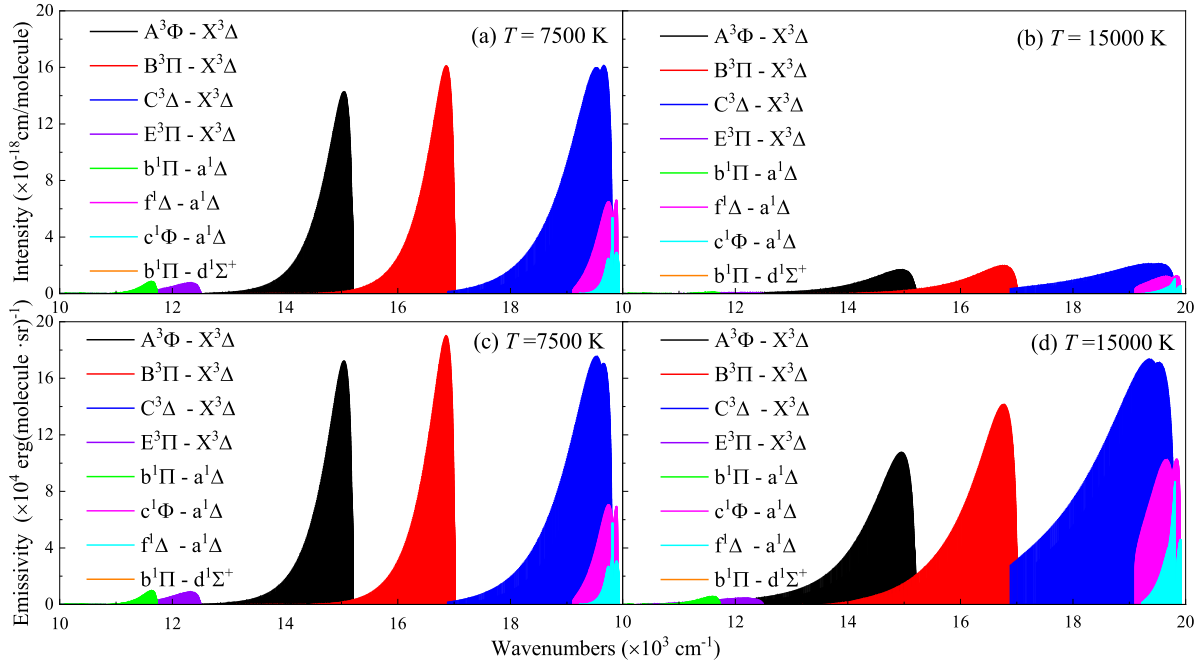
Figure 7. Radiative properties of TiO: (a) absorption line intensity at the temperature of 7500 K, (b) absorption line intensity at the temperature of 15,000 K, (c) emissivity at the temperature of 7500 K and (d) emissivity at the temperature of 15,000 K.
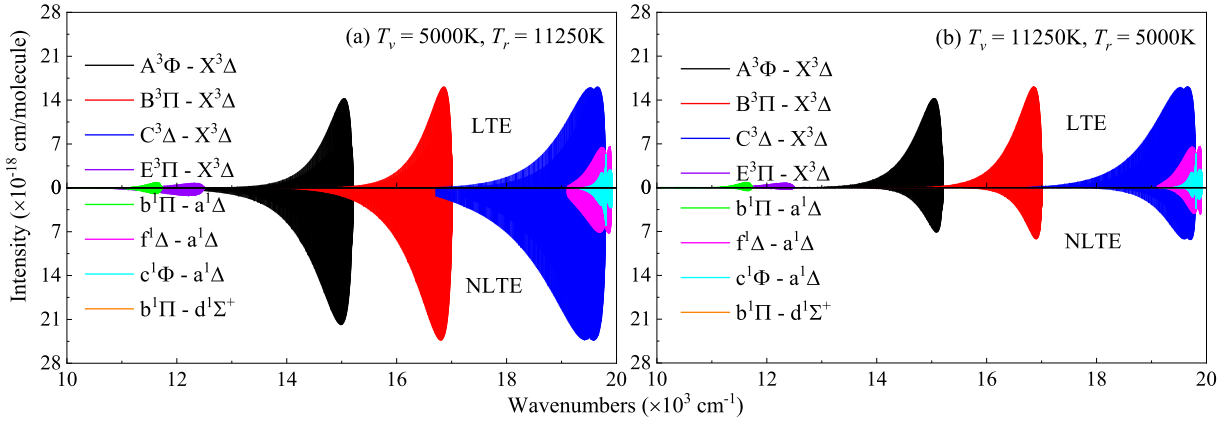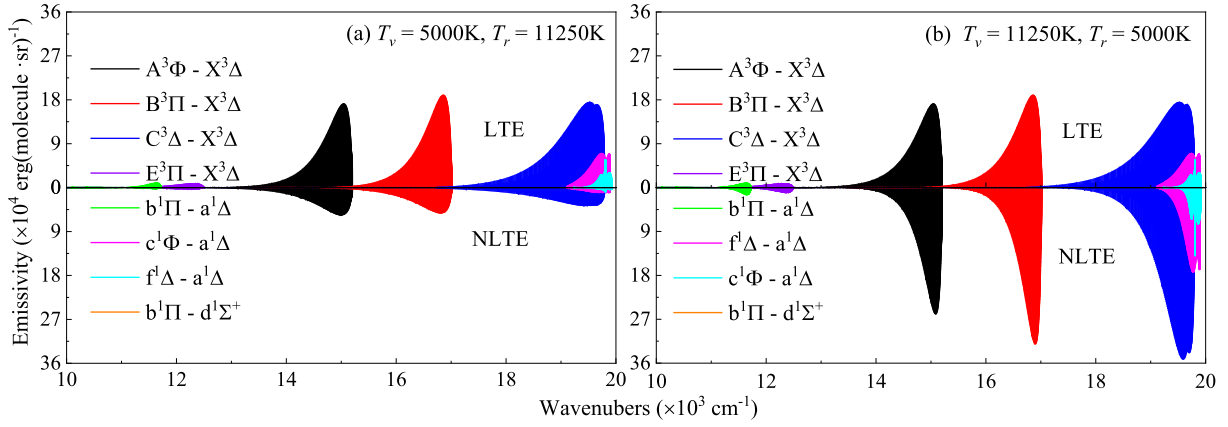

Figure 8. The comparison of the absorption line intensity of TiO by Scheme I in the NLTE and LTE at $T_e = 7500$ K (a) $T_v = 5000$ K and $T_r = 11,250$ K in the NLTE, and (b) $T_v = 11,250$ K and $T_r = 5000$ K in the NLTE.

To understand the effect of the temperature on the absorption and emissivity, we calculated the absorption line intensity and emissivity at the temperatures of 7500 and 15,000 K. For the sake of visual clarity, the absorption line intensity and emissivity of the 0–0 band of each transition are shown in Figure 7. With the temperature increasing, the absorption line intensity decreases obviously but the peak of the emissivity decreases slightly. The effect of the temperature on absorption line intensity is similar to the results of Cheng et al. [11]. In addition, regardless of absorption and emissivity, the higher temperatures cause the spectral lines to broaden, which can be observed in the experiments [41].

3.3.2. Radiative properties in the non-local thermal equilibrium

The gas in the shock layer around the hypersonic vehicles is in the NLTE, thus radiative properties in the NLTE are required. According to the definition of the two-temperature model, the two temperatures (T_v, T_r) in the NLTE have the equivalent temperature T_e, which can be calculated by $T_e = (T_v \, T_r)^{0.5}$. To investigate the effect of the vibrational and rotational temperatures, we calculated the absorption line intensity and emissivity by Scheme I and Scheme II at different T_v and T_r that correspond to the same equivalent temperature 7500 K, as shown in Figures 8–11. For high T_v and low T_r ($T_v >$

Figure 9. The comparison of the emissivity of TiO by Scheme I in the NLTE and LTE at $T_e = 7500$ K (a) $T_v = 5000$ K and $T_r = 11,250$ K in the NLTE, and (b) $T_v = 11,250$ K and $T_r = 5000$ K in the NLTE.
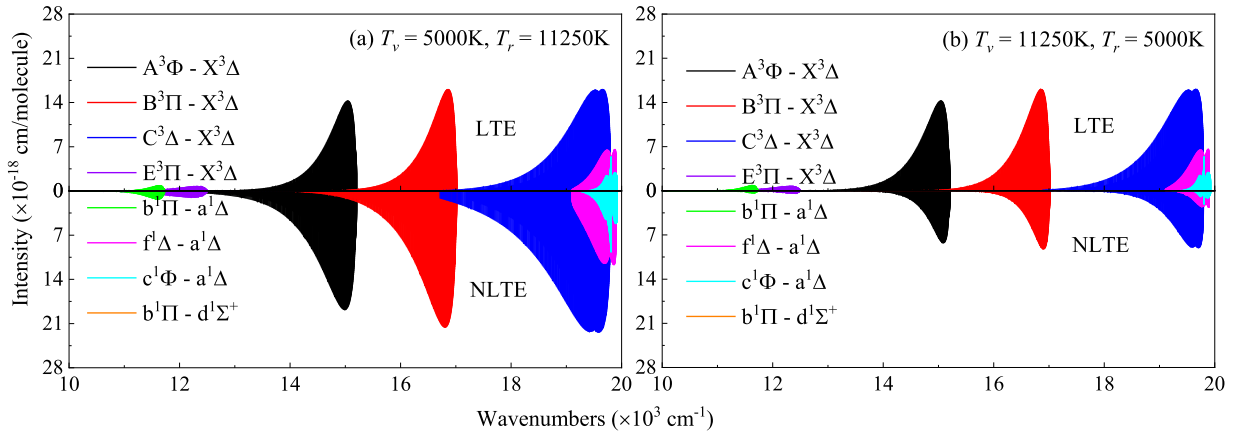
Figure 10. The comparison of the absorption line intensity of TiO by Scheme II in the NLTE and LTE at $T_e = 7500$ K (a) $T_v = 5000$ K and $T_r = 11,250$ K in the NLTE, and (b) $T_v = 11,250$ K and $T_r = 5000$ K in the NLTE.
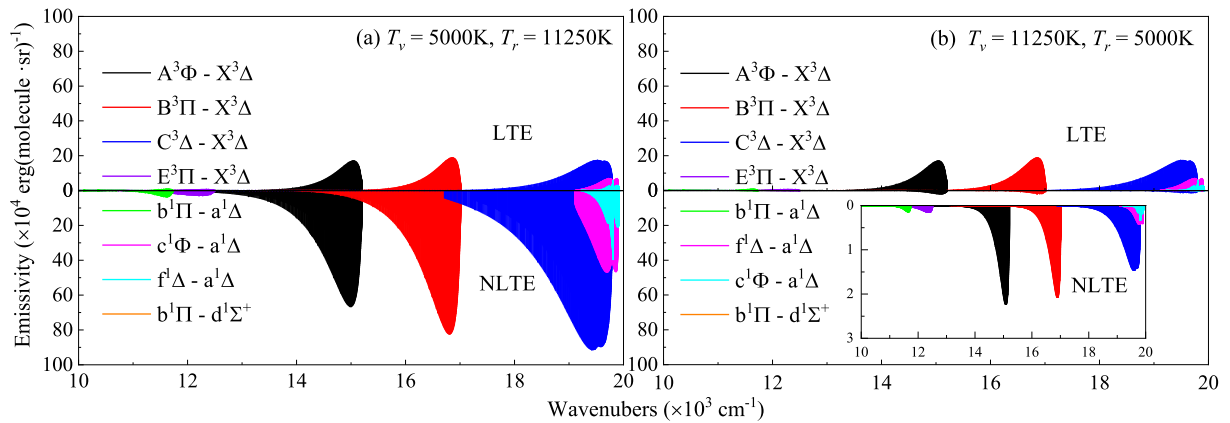
Figure 11. The comparison of the emissivity of TiO by Scheme II in the NLTE and LTE at $T_e = 7500$ K (a) $T_v = 5000$ K and $T_r = 11,250$ K in the NLTE, and (b) $T_v = 11,250$ K and $T_r = 5000$ K in the NLTE.

T_r), the absorption line intensities calculated by Scheme I and Scheme II in the NLTE are lower than those in the LTE. This is due to the higher electronic and vibrational energy contributions for the absorption line intensity. For the emissivity, although it is higher for $T_v >$ T_r by Scheme I and for $T_r < T_v$ by Scheme II, the value by Scheme II is $2 \sim 3$ times larger than those by Scheme I, thus the translational and rotational energy contributes highly to the emissivity. To verify our conclusions, the absorption line intensity and emissivity by

Scheme I and Scheme II at other equivalent temperatures (6000 and 9000 K) were also computed and shown in Figures A.1-8.

4. Conclusions

In this work, the PECs of seven triplets ($X^3\Delta$, $E^3\Pi$, $D^3\Sigma^-$, $A^3\Phi$, $B^3\Pi$, $C^3\Delta$ and $F^3\Sigma^+$) and eight singlets ($a^1\Delta$, $d^1\Sigma^+$, $b^1\Pi$, $1^1\Gamma$, $h^1\Sigma^+$, $2^1\Pi$, $c^1\Phi$ and $f^1\Delta$) of TiO and the TDMs for eight transitions were computed, and then the spectroscopic constants of fifteen electronic states and radiative lifetimes of six states ($A^3\Phi$, $B^3\Pi$, $C^3\Delta$, $b^1\Pi$, $c^1\Phi$ and $f^1\Delta$) were investigated. A large basis set, aug-cc-pwCV5Z-DK, was adopted to compute the PECs of fifteen electronic states by the icMRCI + Q method. Compared with previous theoretical results, the calculated spectroscopic constants and radiative lifetimes are consistent with the earlier experimental and theoretical results.

The fifteen electronic states mentioned above were considered to compute the temperature-dependent IPFs, AIEs and ISHs of TiO in the LTE and NLTE. Our IPFs in the LTE are in good agreement with previous theoretical results. The contributions of different electronic states to the total IPFs in the LTE were also computed to obtain the electronic states that saturate the IPFs at different temperature ranges. For the thermodynamic properties in the NLTE, they were calculated by two energy partitioning schemes, which reveals the IPFs and AIEs are not sensitive to the energy partitioning schemes, but the vibrational and rotational ISHs are strongly affected. The vibrational (rotational) ISHs depend more on the vibrational (rotational) temperature. Due to the higher electronic and vibrational energy contributions, the vibrational ISHs in the Scheme I are largest than other ISHs. Comparing the IPFs in the LTE with those in the NLTE, the condition of the gas (LTE or NLTE) may have no effect on the contributions of a specific electronic state to the total IPFs and the saturation of electronic states at different temperatures.

Eight transitions were considered to compute the absorption line intensity and emissivity of TiO in the LTE and NLIE at the equivalent temperatures of 6000, 7500 and 9000 K. The $A^3\Phi-X^3\Delta$, $B^3\Pi-X^3\Delta$ and $C^3\Delta-X^3\Delta$ transitions play a key role in the calculations of the absorption and emissivity, where our calculated strongest line position in the $C^3\Delta-X^3\Delta$ system is close to the measured value in the experiments. With the temperature increasing, the absorption line intensity decreases obviously but the peak of the emissivity decreases slightly. For the radiative properties in the NLTE, the results show the higher electronic and vibrational energy contributions for the absorption line intensity and the higher translational and rotational energy contributions for the emissivity.

The calculated thermodynamic and radiative data in the LTE and NLTE of TiO in this paper can be used to predict the heat load of aircrafts and provide guidance for the design of the thermal protection system.

Credit authorship contribution statement

Tianrui Bai: Software, Investigation, Conceptualisation, Methodology, Writing-Original Draft.
Zhi Qin: Investigation, Conceptualisation, Data curation, Review & Editing.
Linhua Liu: Supervision, Funding acquisition, Conceptualisation, Data curation, Review & Editing.

ORCID

Zhi Qin (iD) http://orcid.org/0000-0001-7995-0006

References

[1] Q. Niu, Z. Yuan, B. Chen and S. Dong, Chinese J. Aeronaut. 32, 861–874 (2019). doi:10.1016/j.cja.2019.01.003
[2] Y. Zeng, X. Xiong, G. Li, Z. Chen, W. Sun and D. Wang, Carbon. N. Y. 54, 300–309 (2013). doi:10.1016/j.carbon.2012.11.042
[3] P. Makurunje, F. Monteverde and I. Sigalas, J. Eur. Ceram. Soc. 37 (10), 3227–3239 (2017). doi:10.1016/j.jeurceramsoc.2017.03.068
[4] L. Ran, K. Peng, M. Yi and L. Yang, Mater. Lett. 65 (13), 2076–2078 (2011). doi:10.1016/j.matlet.2011.04.017
[5] H. Wu, M. Yi, Y. Ge, K. Peng and L. Ran, Corros. Sci. 160, 108175 (2019). doi:10.1016/j.corsci.2019.108175
[6] Z. Qin, J.M. Zhao and L.H. Liu, J. Quant. Spectrosc. Radiat. Transf. 210, 1–18 (2018). doi:10.1016/j.jqsrt.2018.02.004
[7] M. Panesi, *Pise: Università di Pisa* (2009)
[8] L.K. McKemmish, T. Masseron, H.J. Hoeijmakers, V. Pérez-Mesa, S.L. Grimm, S.N. Yurchenko and J. Tennyson, Mon. Not. Roy. Astron. Soc. 488 (2), 2836–2854 (2019). doi:10.1093/mnras/stz1818
[9] D.W. Schwenke, Faraday Discuss. 109, 321–334 (1998). doi:10.1039/a800070k
[10] J.B. Tatum, Publ. Dom. Astrophys. Obs. 13 (1), 1 (1966).

[11] J. Cheng, H. Zhang, X. Cheng, J. Wang and S. Wu, J. Mol. Spectrosc. 371, 111325 (2020). doi:10.1016/j.jms.2020.111325.

[12] W.Z. Wang, M.Z. Rong, J. Yan, A. Murphy and J.W. Spencer, Phys. Plasmas. 18 (11), 113502 (2011). doi:10.1063/1.3657426

[13] D. Bruno, M. Capitelli, C. Catalfamo and A. Laricchiuta, Phys. Plasmas. 15, 112306 (2008). doi:10.1063/1.3012566

[14] R. Ram, P. Bernath and L. Wallace, Astrophys. J. Suppl. S. 107, 443 (1996). doi:10.1086/192370

[15] L.A. Kaledin, J.E. McCord and M.C. Heaven, J. Mol. Spectrosc. 173 (2), 499–509 (1995). doi:10.1006/jmsp.1995.1252

[16] W.H. Hocking, M. Gerry and A. Merer, Can. J. Phys. 57 (1), 54–68 (1979). doi:10.1139/p79-006

[17] C.N. Kei-ichi, H. Ito and S.P. Davis, J. Mol. Spectrosc. 217 (2), 173–180 (2003). doi:10.1016/S0022-2852(02)00027-9

[18] C. Amiot, M. Cheikh, P. Luc and R. Vetter, J. Mol. Spectrosc. 179 (1), 159–167 (1996). doi:10.1006/jmsp.1996.0194

[19] K. Kobayashi, G.E. Hall, J.T. Muckerman, T.J. Sears and A.J. Merer, J. Mol. Spectrosc. 212 (2), 133–141 (2002). doi:10.1006/jmsp.2002.8543

[20] R. Ram, P. Bernath, M. Dulick and L. Wallace, Astrophys. J. Suppl. S. 122 (1), 331–353 (1999). doi:10.1086/313212

[21] E. Miliordos and A. Mavridis, J. Phys. Chem. A. 114 (33), 8536–8572 (2010). doi:10.1021/jp910218u

[22] A.N. Smirnov, V.G. Solomonik, S.N. Yurchenko and J. Tennyson, Phys. Chem. Chem. Phys. 21 (41), 22794–22810 (2019). doi:10.1039/C9CP03208H

[23] H.J. Werner and P.J. Knowles, J. Chem. Phys. 82 (11), 5053–5063 (1985). doi:10.1063/1.448627

[24] P.J. Knowles and H.-J. Werner, Chem. Phys. Lett. 115 (3), 259–267 (1985). doi:10.1016/0009-2614(85)80025-7

[25] P.J. Knowles and H.-J. Werner, Chem. Phys. Lett. 145 (6), 514–522 (1988). doi:10.1016/0009-2614(88)87412-8

[26] K. P. J. Werner H.-J., Knizia G., Manby F.R., others a. MOLPRO, a package of ab initio programs, see < http://www.molpronet > (2015).

[27] R.J. Le Roy, J. Quant. Spectrosc. Radiat. Transf. 186, 167–178 (2017). doi:10.1016/j.jqsrt.2016.05.028

[28] D.C. Galehouse, S.P. Davis and J.W. Brault, Astrophys. J. Suppl. S. 42, 241–259 (1980). doi:10.1086/190650

[29] J.G. Phillips, Astrophys. J. Suppl. S. 26, 313–331 (1973). doi:10.1086/190283

[30] R. JAFFE, Presented at the 22nd Thermophysics Conference, 1987 (unpublished).

[31] S.N. Yurchenko, A.F. Al-Refaie and J. Tennyson, Astron. Astrophys. 614, A131 (2018). doi:10.1051/0004-6361/201732531

[32] G.R. Brandes and D.C. Galehouse, J. Mol. Spectrosc. 109, 345–351 (1985). doi:10.1016/0022-2852(85)90317-0

[33] M. Barnes, A. Merer and G. Metha, J. Mol. Spectrosc. 181 (1), 180–193 (1997). doi:10.1006/jmsp.1996.7161

[34] C. Amiot, P. Luc and R. Vetter, J. Mol. Spectrosc. 214 (2), 196–201 (2002). doi:10.1006/jmsp.2002.8592

[35] I. Hedgecock, C. Naulin and M. Costes, Astron. Astrophys. 304, 667–677 (1995).

[36] J. Schamps, J. Sennesal and P. Carette, J. Quant. Spectrosc. Radiat. Transf. 48 (2), 147–152 (1992). doi:10.1016/0022-4073(92)90084-H

[37] S. R. Langhoff, Astrophys. J. 481 (2), 1007–1015 (1997). doi:10.1086/304077

[38] M. Doverstål and P. Weijnitz, Mol. Phys. 75 (6), 1357–1363 (1992). doi:10.1080/00268979200101031

[39] Y. Babou, P. Rivière, M. Y. Perrin and A. Soufiani, Int. J. Thermophys. 30 (2), 416–438 (2009). doi:10.1007/s10765-007-0288-6

[40] T. Gustavsson, C. Amiot and J. Vergès, J. Mol. Spectrosc. 145 (1), 56–65 (1991). doi:10.1016/0022-2852(91)90350-J

[41] D.D. Lee, F.A. Bendana, A.P. Nair, D.I. Pineda and R.M. Spearrin, J. Quant. Spectrosc. Radiat. Transf. 253, 107135 (2020). doi:10.1016/j.jqsrt.2020.107135